J. Fluid Mech. (2006), *vol.* 556, *pp.* 1–25.
doi:10.1017/S0022112006009141 Printed in the United Kingdom

The linear stability of high-frequency oscillatory flow in a channel

By P. J. BLENNERHASSETT[1] AND ANDREW P. BASSOM[2]

[1]School of Mathematics, University of New South Wales, Sydney 2052, Australia
[2]School of Mathematics and Statistics, University of Western Australia, Crawley 6009, Australia

(Received 17 April 2005 and in revised form 2 November 2005)

The linear stability of the Stokes layers generated between a pair of synchronously oscillating parallel plates is investigated. The disturbance equations were studied using Floquet theory and pseudospectral numerical methods used to solve the resulting system. Neutral curves for an extensive range of plate separations were obtained and when the plate separation is large compared to the Stokes layer thickness the linear stability properties of the Stokes layer in a semi-infinite fluid were recovered. A detailed analysis of the damping rates of disturbances to the basic flow provides a plausible explanation of why several previous studies of the problem have failed to detect any linear instability of the flow.

To compare more faithfully with experimental work the techniques used for the channel problem were modified to allow the determination of neutral curves for axisymmetric disturbances to purely oscillatory flow in a circular pipe. Critical Reynolds numbers for the pipe flow tended to be smaller than their counterparts for the channel case but the smallest critical value was still almost twice the experimentally reported result.

1. Introduction

The flow generated in a semi-infinite layer of a viscous fluid when the bounding infinite flat plate oscillates in its own plane is generally referred to as a Stokes layer (von Kerczek & Davis 1974). This flow is the prototype unsteady viscous boundary layer and some form of Stokes layer occurs on the bounding surfaces of many high-frequency oscillatory flows. In particular, purely oscillatory motion in pipes and channels can be decomposed into an inviscid flow away from the walls with a Stokes layer adjacent to the boundaries, provided the frequency of oscillation is sufficiently large. Flows meeting this condition occur in a variety of industrial and physiological situations – some examples are given in Hale, McDonald & Womersley (1955), Ku (1997), Selverov & Stone (2001) and Suresh & Homsy (2004). It is undeniable that the stability properties of Stokes layers are of both practical and theoretical interest.

From a theoretical point of view the planar Stokes layer is a paradigm for purely oscillatory parallel flows and several attempts have been made to predict its linear stability properties. Stokes layers are characterized by three dimensional quantities: the frequency of the oscillations, ω, the amplitude of the fluid velocity, U_0 (either at the wall or within the inviscid core) and the kinematic viscosity, ν, of the fluid. These quantities combine to form the Reynolds number

$$R = U_0/\sqrt{2\nu\omega},$$

which is the main parameter determining the stability of the Stokes layer. Experimental work has clearly demonstrated that the flow is unstable at sufficiently large Reynolds numbers (see, for example, Akhavan, Kamm & Shapiro (1991*a*) for a summary of some relevant work) but the wide variation in reported results means that there is no agreed definitive value of R characterizing the onset of instability. Depending on the experimental apparatus used, values of R ranging from 140 to 270 have been suggested for the stage at which the basic laminar Stokes layer loses stability. In contrast to the experimental evidence, the early theoretical approaches failed to detect any linear instability at all. Indeed, for high-frequency oscillatory flow in a channel, the results of von Kerczek & Davis (1974) showed that for R up to 400 the least-stable disturbance mode actually becomes more stable as R increases. Although they examined a slightly different problem, the calculations of Akhavan, Kamm & Shapiro (1991*b*) essentially confirmed the results of von Kerczek & Davis, at least as far as the linear stability of the flow is concerned. Moreover, for the case of a Stokes layer bounding a semi-infinite layer of fluid, the study of Hall (1978) could not detect any linear instability for $R < 160$.

All the theoretical investigations described above are rational in the sense that no restrictions were imposed on the temporal dependence of the perturbations beyond the assumption that they satisfy the normal linear stability equations supplemented by appropriate boundary conditions. In contrast, some studies of the stability of Stokes layers at finite Reynolds numbers have used *ad-hoc* conditions which assert that the disturbance should change much more rapidly than the underlying flow. This constraint leads to an easier theoretical task but such 'quasi-steady' formulations can give rise to several possible definitions of instability. Furthermore, von Kerczek & Davis (1974) have argued that these quasi-steady approaches are flawed, and to date there has been no rigorous mathematical justification for the approximations made. The assumptions of the finite Reynolds number, 'quasi-steady' approach to the linear instability of Stokes layers are further undermined by the results of Akhavan *et al.* (1991*b*). By numerically solving the linear initial value problem governing the evolution of disturbances in oscillatory flow in a channel, Akhavan *et al.* (1991*b*) showed that there was no rapid growth phase for disturbances, even at Reynolds numbers where turbulence in the basic flow had been reported. On the other hand, rational quasi-steady stability calculations for purely oscillatory plane flows are possible as the Reynolds number tends to infinity (Cowley 1987; de Souza 1998). For the case of a Stokes layer bounding a semi-infinite flow Hall (2003) has used a quasi-steady analysis to demonstate the existence of disturbances with periodic growth rates, provided the disturbance wavenumber is above a certain critical value. However our interest is in the initial instability of the basic flow, which occurs at a finite Reynolds number, and consequently only stability calculations based on Floquet theory, as in von Kerczek & Davis (1974) or Hall (1978), or initial value problems (Akhavan *et al.* 1991*b*) will be considered here.

The most recent work on the linear stability of plane Stokes layers appears to be that of Blennerhassett & Bassom (2002), hereafter referred to as BB. Their calculations followed the method detailed by Hall (1978) who showed that a semi-analytical solution of the governing equations was possible. Hall's method leads to the computational problem of locating the zeros of a (formally infinite) determinant as a function of the disturbance growth rate. As the size of the finite-dimensional truncation of the determinant grew with increasing R, the computational resources available at the time meant that Hall (1978) was not able to take his work beyond $R = 160$ and hence was unable to find any evidence of instability. But BB, aided by

greater computational resources and some refined numerical methods, were able to locate the linear stability neutral curve. In particular they identified a critical Reynolds number of approximately 708 for the oscillatory boundary layer on an infinite flat plate in a semi-infinite layer of fluid. Nevertheless computational constraints could not be avoided altogether so that BB were unable to investigate some interesting aspects of the stability of the flow. In particular their results were inconclusive regarding the fate of the instability modes as $R \to \infty$. The subsequent study by Hall (2003) concluded that the Stokes layer reverts to being linearly stable in the formal high-Reynolds-number limit.

Given the general expectation that the stability properties of a Stokes layer in a wide channel should approximate those in a semi-infinite layer (von Kerczek & Davis 1974) there is clear potential conflict between the linear instability results of BB (for large enough R) and the increasing stability predictions of von Kerczek & Davis (1974) described earlier. In an attempt to resolve these contradictions, while simultaneously providing an independent check of the results in BB, the linear stability of high-frequency oscillatory flow in a finite-width channel is examined in this paper. The semi-analytical technique of Hall (1978) used by BB does not generalize easily to oscillatory flow in a finite-width channel and so a purely numerical method is used to solve the equations obtained from a Floquet decomposition of the perturbations to the basic flow. Thus the stability results obtained using this approach are completely independent of the assumptions underlying the calculations in BB. The main finding is that for R less than about 400 the results to be given here agree qualitatively with those of von Kerczek & Davis (1974), who examined a slightly different basic flow from that considered here. Moreover, at larger values of R, the present results agree quantitatively with those in BB, provided the channel width is large enough.

The Stokes layer thickness, $\sqrt{2\nu/\omega}$, provides a characteristic length scale for the flow, so that if the dimensional channel width is $2d$ then the scaled channel half-width parameter is $h \equiv d/\sqrt{2\nu/\omega}$. Our results show that oscillatory flow in a channel has essentially the same critical conditions for instability as the semi-infinite Stokes layer flow provided that h is greater than about 14. We note in passing that Akhavan *et al.* (1991*b*) considered a flow with $h = 10$ and von Kerczek & Davis (1974) effectively took $h = 8$; both these investigations chose channel widths which were hoped to be sufficiently large to provide very good approximations to the semi-infinite Stokes layer. Given the way that the flow in this layer decays exponentially with distance from the bounding plate it would seem that $h = 8$ would be ample for the purposes required. It is of some surprise that both Akhavan *et al.* (1991*b*) and von Kerczek & Davis (1974) would have been unable to draw detailed quantitative conclusions regarding the stability of a semi-infinite Stokes layer.

Much experimental work conducted to assess the stability of plane Stokes layers is, in practice, actually carried out in circular pipes (examples include Hino, Sawamoto & Takasu 1976; Clamen & Minton 1977; Eckmann & Grotberg 1991) rather than channels. Practically, it is difficult to generate a flat Stokes layer but rather less complicated to obtain accurate oscillatory flows in pipes. Consequently, in order to ease the comparison of our theoretical predictions of instability with available experimental results, the stability of oscillatory flow in a pipe is also considered here. The calculations for the pipe are based on a simple extension of the techniques used for two-dimensional disturbances in a channel and only axisymmetric disturbances to the pipe flow are examined. For a sufficiently large pipe radius the results of BB are again retrieved, but when the (non-dimensional) pipe radius is about 10 there is a minimum, of approximately 570, in the critical Reynolds number. While this

predicted critical Reynolds number is less than that obtained in BB for the plane semi-infinite layer, it is still much larger than the experimentally observed value.

The remainder of this work is organized as follows. The governing linear stability equations are derived in § 2 where the numerical methods are also discussed. Detailed results for the channel flow are described in § 3 while the extension to the stability of axisymmetric disturbances to oscillatory flow in a circular pipe is considered in § 4. The paper concludes with some discussion of practical implications of our results.

2. Formulation and numerical methods

Consider the motion induced in a Newtonian fluid by synchronously oscillating two infinite parallel plates, a distance $2d$ apart, with the velocity $U_0 \cos \omega t$. If each plate oscillates in its own plane and there are no disturbances, a uni-directional flow with the fluid velocity parallel to the plates is generated. A dimensionless form for this basic flow is obtained if all lengths are scaled on $\sqrt{2\nu/\omega}$, all velocity components on U_0 and the non-dimensional time $\tau = \omega t$ is introduced. If the movement of the plates is in the x-direction, with the y-direction normal to the bounding surfaces, the undisturbed basic flow takes the form

$$u = U_B(y, \tau) = \mathrm{Re}\left\{ \frac{\cosh((1+\mathrm{i})y)}{\cosh((1+\mathrm{i})h)} \mathrm{e}^{\mathrm{i}\tau} \right\} = u_1(y)\mathrm{e}^{\mathrm{i}\tau} + u_{-1}(y)\mathrm{e}^{-\mathrm{i}\tau}, \quad v = w = 0, \quad (2.1)$$

where the velocity vector $\boldsymbol{u} = (u, v, w)$ has components corresponding to the coordinates (x, y, z). The half-width of the channel is $h = d\sqrt{\omega/2\nu}$, so that for high-frequency oscillations h measures the separation of the plates in terms of the thickness of the Stokes layers formed at the channel walls. We note that for h greater than about 2π the vorticity generated by the movement of the walls is unable to diffuse to the centre of the channel and the basic flow is then effectively zero around $y = 0$. Thus, as we are primarily interested in the linear stability of high-frequency oscillatory flows which have Stokes layers bounding an essentially inviscid core flow, we only consider values of h greater than about 5.

The linear stability of the basic flow (2.1) is found by considering a disturbed flow in the form

$$(u, v, w) = (U_B, 0, 0) + \varepsilon \left(\frac{\partial \Psi}{\partial y}, -\frac{\partial \Psi}{\partial x}, 0 \right), \quad (2.2)$$

where $\varepsilon \ll 1$ and Ψ denotes the stream function of a two-dimensional disturbance. As Squire's theorem has been extended to unsteady flows (Conrad & Criminale 1965; von Kerczek & Davis 1974) the above perturbation is sufficient to locate the critical conditions for linear instability. The disturbance stream function is further decomposed to expose explicitly any exponential growth with time by seeking Floquet solutions in the form

$$\Psi = \mathrm{e}^{\mu\tau}\mathrm{e}^{\mathrm{i}ax}\psi(y, \tau) + \text{complex conjugate}, \quad (2.3)$$

where $\psi(y, \tau)$ is taken to be 2π-periodic in τ with any exponential growth or decay of Ψ incorporated in μ. With this form for the velocity field the linearized equation for ψ is then

$$\frac{\partial}{\partial \tau}\left(\frac{\partial^2}{\partial y^2} - a^2 \right)\psi = \left\{ \frac{1}{2}\left(\frac{\partial^2}{\partial y^2} - a^2 \right) - \mu - \mathrm{i}aRU_B \right\}\left(\frac{\partial^2}{\partial y^2} - a^2 \right)\psi + \mathrm{i}aRU_{B_{yy}}\psi, \quad (2.4)$$

subject to

$$\psi = \psi_y = 0 \quad \text{on} \quad y = \pm h. \quad (2.5)$$

As in BB the wavenumber a is real and the growth rate μ is complex, while the symmetries of the equation allow all solutions to be obtained by restricting the imaginary part of μ to the interval $\mu_i \in [0, \frac{1}{2}]$. The unknown function ψ was decomposed into harmonics

$$\psi = \sum_{n=-\infty}^{\infty} \psi_n(y) \mathrm{e}^{\mathrm{i}n\tau},$$

so that equating coefficients of the harmonics in (2.4) results in the infinite system of ordinary differential equations

$$\left(\frac{\partial^2}{\partial y^2} - a^2 - 2\mu - 2\mathrm{i}n\right)\zeta_n = 2\mathrm{i}aR[(\zeta_{n-1} - 2\mathrm{i}\psi_{n-1})u_1 + (\zeta_{n+1} + 2\mathrm{i}\psi_{n+1})u_{-1}], \quad (2.6a)$$

$$\left(\frac{\partial^2}{\partial y^2} - a^2\right)\psi_n = \zeta_n \quad (2.6b)$$

where the spatial derivatives of the basic flow have been simplified using the relationship that $u_{1yy} = 2\mathrm{i}u_1$ and ζ_n is just an abbreviation for the Laplacian of ψ_n. Analogous systems have been used by Hall (1978) and BB.

The numerical solution of the system (2.6) was obtained using the pseudospectral techniques described by Fornberg (1996) and Trefethen (2000). Each differential operator appearing in the governing equations was replaced by its pseudospectral matrix approximation, with each $\psi_n(y)$ being represented by a vector $\boldsymbol{\psi}_n$ of its function values on a Chebyshev mesh on the interval $-h \leqslant y \leqslant h$. Thus a discrete approximation to the equations (2.6) can be written as

$$-\mathrm{i}aR\widetilde{\boldsymbol{M}}\boldsymbol{\psi}_{n+1} + (\boldsymbol{L}^{-1}\boldsymbol{V} - \mathrm{i}n\boldsymbol{I})\boldsymbol{\psi}_n - \mathrm{i}aR\boldsymbol{M}\boldsymbol{\psi}_{n-1} = \mu\boldsymbol{\psi}_n, \quad (2.7)$$

for each integer n. Here $\boldsymbol{I}$ is the appropriately sized identity matrix and $\boldsymbol{L}$, $\boldsymbol{V}$ and $\boldsymbol{M}$ are pseudospectral differentiation matrices representing the continuous operators:

$$\partial_y^2 - a^2 \to \boldsymbol{L}, \quad \left(\partial_y^4 - 2a^2\partial_y^2 + a^4\right)/2 \to \boldsymbol{V}, \quad \boldsymbol{M} = \boldsymbol{L}^{-1}u_1(\boldsymbol{L} - 2\mathrm{i}\boldsymbol{I}). \quad (2.8)$$

Finally, $\widetilde{\boldsymbol{M}}$ denotes the complex conjugate of $\boldsymbol{M}$ and, allowing for an obvious abuse of notation, u_1 in (2.8) denotes the square matrix with the mesh values of $u_1(y)$ down the diagonal.

The boundary condition requiring no flow through the channel walls was implemented by omitting the first and last equation, for each n, from (2.7) while the no-slip condition, $\psi_{ny}(\pm h) = 0$, was enforced using the procedure described by Trefethen (2000). This method is based on the observation that the kinematic condition $\psi_n(\pm h) = 0$ requires that ψ_n has the form $(h^2 - y^2)g_n(y)$, so that the no-slip condition can then be imposed by demanding $g_n(\pm h) = 0$. A transformation from ψ_n to g_n and then back to ψ_n is built into the differentiation matrices (Trefethen 2000, chapter 14), so that both boundary conditions at $y = \pm h$ can be imposed by dropping just one equation at each boundary. Further, this no-slip condition was not used in all spectral differentiation matrices, but was incorporated into the pseudo-spectral approximation to ∂_y^4, as suggested by Trefethen (2000), and used previously elsewhere (Fornberg 1996). Thus, if the domain $[-h, h]$ is divided into $2K$ subintervals, equation (2.7) represents $2K - 1$ algebraic equations for the values of ψ_n at the internal mesh points. As the basic flow is an even function of y and as there are only even-order differential operators in the governing equation (2.4), the solution set for $\psi_n(y)$ can be decomposed into functions even in y and functions which are odd in y. When this symmetry is applied to the discrete variable $\boldsymbol{\psi}_n$, we find that the odd modes require

only $K-1$ unknowns and the solutions even in y need only K function values. A finite system of algebraic equations was obtained by truncating the Fourier series for $\psi(y,\tau)$ and setting $\psi_n = 0$ for $|n| > N$, where N was typically two to three hundred when locating the neutral conditions. With the vector $\boldsymbol{\Phi}$ defined by

$$\boldsymbol{\Phi}^T = \left(\boldsymbol{\psi}_N^T \quad \boldsymbol{\psi}_{N-1}^T \ldots \boldsymbol{\psi}_0^T \ldots \boldsymbol{\psi}_{-N}^T\right) \tag{2.9}$$

the system (2.7) becomes the eigenvalue problem

$$\boldsymbol{A}\boldsymbol{\Phi} = \mu\boldsymbol{\Phi} \tag{2.10}$$

where $\boldsymbol{A}$ is a sparse, block diagonal matrix with $(2N+1)(K-1)$ (odd modes) or $(2N+1)K$ (even modes) rows and columns. The $(\boldsymbol{L}^{-1}\boldsymbol{V} - \mathrm{i}n\boldsymbol{I})$ blocks appear along the diagonal of $\boldsymbol{A}$, with the $-\mathrm{i}a R\boldsymbol{M}$ blocks above the diagonal and the $-\mathrm{i}a R\widetilde{\boldsymbol{M}}$ blocks below it.

The eigenvalues μ and eigenvectors $\boldsymbol{\Phi}$ of the discrete system (2.10) were found using the sparse matrix eigenvalue routines in Matlab. A range of checks were applied to the results of these calculations to ensure that the solutions were independent of the parameters N and K controlling the discrete approximation to the underlying continuous system. For Reynolds numbers in the range 500 to 1000 values for μ accurate to more than five significant figures could easily be obtained using $K \approx 50$. Progressively increasing K rapidly increases the number of significant figures in the eigenvalues obtained, as is expected with a spectral approximation scheme. At very large values of R and n, say $R \approx 3000$ and $n \approx 300$, plots of the eigenfunctions $\boldsymbol{\psi}_n$ as functions of y sometimes appeared a little ragged for $K \approx 50$. However, increasing the value of K only made tiny changes to the eigenvalue while resolving the oscillations in the eigenfunctions with large n. The concentration of points in the Chebyshev mesh near $y = \pm h$ allowed accurate resolution of any wall layers, while leaving sufficient density of points just outside the basic Stokes layer where the eigenfunctions assumed their largest size. Graphs showing the structure of some of the larger eigenfunctions $\psi_n(y)$ at $R = 700$ with $a = 0.3$ and $h = 16$ are shown later, where the properties of the $\psi_n(y)$ are also discussed more fully. Most of the results presented below were obtained using $K = 48$.

The number of harmonics N retained in the Fourier representation of $\psi(y,\tau)$ had a very strong influence on the accuracy of the eigenvalue μ associated with the unstable disturbance modes. With N too small the real part of the eigenvalue μ_r was overestimated; this behaviour was reported by Hall (1978) and also noted by BB. In fact the dependence of μ on N observed in this work was practically identical to that detailed in BB, and so will not be discussed further. However, the routines used within Matlab allowed checks on the accuracy of μ (additional to those undertaken in BB) to be easily performed. Given an eigenvalue γ, the symmetries in the governing equations (2.4) show that $\mu = \gamma + \mathrm{i}k$, for any integer k, is also an eigenvalue. If too few harmonics were used then this property of the exact eigenvalues was not accurately replicated by the eigenvalues found from the Matlab routines applied to the discrete system (2.10). For values of R from zero to just above the neutral curve, it was found empirically that provided N was greater than approximately $0.8aR$ the value of μ was accurate to at least five significant figures and independent of N. This is again similar to the results of checks described in BB.

The determination of the eigenvector $\boldsymbol{\Phi}$ became problematic when N exceeded about 120. The exponential decay of $|\psi_n|$ with increasing $|n|$ caused the size of the harmonics in the tail of the Fourier series to fall below the built-in convergence tolerances of the Matlab routines, and hence produce noise, around a mean value of

about 10^{-16}, in the vectors $\boldsymbol{\psi}_n$ with $|n|$ close to N. This difficulty was overcome by redefining $\boldsymbol{\Phi}$ as

$$\boldsymbol{\Phi}^T = \left(\lambda^{-N}\boldsymbol{\psi}_N^T \quad \lambda^{-N+1}\boldsymbol{\psi}_{N-1}^T \quad \ldots \boldsymbol{\psi}_0^T \ldots \lambda^{-N}\boldsymbol{\psi}_{-N}^T\right) \tag{2.11}$$

so that with $\lambda > 1$ some of the exponential decay of the Fourier coefficients is automatically included and the size of the rescaled $\boldsymbol{\psi}_n$ will not decrease as rapidly with increasing $|n|$. This change in the definition of $\boldsymbol{\Phi}$ induces a similarity transformation of the matrix $\boldsymbol{A}$ appearing in (2.10) and hence does not alter the eigenvalues of the system. The values of λ needed to absorb the decay of the harmonics were generally in the range $1.02 < \lambda < 1.1$, depending on the value of N and the parameters a and R, and successful computation of eigenvectors was obtained, even when the size of the unscaled $\boldsymbol{\psi}_{\pm N}$ of (2.9) was $O(10^{-30})$.

A final check on the internal self-consistency of the numerical procedures was provided by verifying that the solution obtained from (2.10), which is essentially a problem in the frequency domain, actually satisfied the original governing equation (2.4) in the time domain. Fast Fourier transform routines were used to reconstruct the values of ψ and ψ_τ at points (y_k, τ_n), where the y_k are the points in the Chebyshev mesh on $0 < y < h$ and $\tau_n = 2n\pi/(2N+1)$ with $0 \leqslant n \leqslant 2N$. Spectral differentiation matrices were again used to approximate the spatial derivatives in (2.4). As the derivation of the eigenvalue problem (2.10) involved the application of the inverse of a Laplacian operator, and the check of the governing equation did not, there is some degree of independence in the verification of the spatial derivatives. When this check was carried out for parameter values close to the neutral curve, the maximum error in the governing equation was always a factor of $O(10^{-7})$ smaller than the maximum of the viscous terms in the equation, with this maximum error occurring only for a few mesh points close to the wall. Over most of the flow domain the error was smaller than the maximum error by at least another five orders of magnitude.

The procedures described above cover the internal consistency of the numerical approximations used to obtain the stability properties of the basic flow. Further verification of our results was provided by comparison with known results for special limits of the governing equations and previously published data; this is discussed in the next section.

3. Results

At small Reynolds numbers an analytical solution of the governing equations (2.4) can be found in the form

$$\psi_n \sim R^n(\psi_{n0} + R^2\psi_{n2} + \cdots) \quad \text{with} \quad \mu \sim \mu_0 + R^2\mu_2 + \cdots \tag{3.1}$$

(Dolph & Lewis 1958) where the eigenvalue μ_0 comes from the solution of the transcendental equation

$$(\gamma \tan \gamma h + a \tanh ah)(\gamma \tanh ah - a \tan \gamma h) = 0 \quad \text{where } \gamma^2 = -a^2 - 2\mu. \tag{3.2}$$

There is an infinite family of real eigenvalues μ_{0j}^e corresponding to the even eigenfunctions

$$\psi_{00} = \phi_{0j}^e(y) = \frac{\cosh ay}{\cosh ah} - \frac{\cos \alpha^e y}{\cos \alpha^e h}, \qquad \alpha^e \equiv \sqrt{-a^2 - 2\mu_{0j}^e},$$

and an analogously defined family of odd eigenfunctions $\psi_{00} = \phi_{0j}^o(y)$ with real eigenvalues μ_{0j}^o. The μ_{0j}^e values arise from the zeros of the first factor in (3.2) and the

	$R=0.1$		$R=570$		$R=750$	
h	even	odd	even	odd	even	odd
8	−0.08833	−0.18181	−0.54130	−0.94410		
16	−0.05249	−0.07339	−0.06572	−0.11620	−0.06695	−0.11951

TABLE 1. Values of μ for the least damped even and odd modes for $a=0.3$ and various values of R and h. Note that for the indicated parameter values μ is purely real.

μ_{0j}^{o} from the zeros of the second factor. At $R=0$ the values for μ obtained by the numerical method described in §2 agreed with the Dolph–Lewis eigenvalues μ_{0j}^{e} or μ_{0j}^{o} to more than ten figures for the cases h equal to 1, 8 and 16 with a wavenumber of 0.3 or 0.4; the first eigenvalue was checked in all cases with sporadic checks made on modes up to the tenth.

The results of von Kerczek & Davis (1974) for Reynolds numbers up to 400 (in our scaling) showed that their principal Floquet exponent was always real and became more negative as R increased from zero, indicating that the basic flow becomes more stable with increasing R. For the basic flow considered here, analogous results were obtained for the μ with largest real part over the Reynolds number range given in table 1. These damping rates of the perturbations for the least stable even and odd perturbations, for both values of the channel half-width, clearly agree with the trend found by von Kerczek & Davis (1974). The above results are consistent qualitatively with the calculations reported by Akhavan *et al.* (1991*b*) for the case of $h=10$. Their direct integration in time of (2.4), treated as an initial value problem, showed that all disturbances decayed to zero for Reynolds numbers up to 500. After some possible initial growth, due to the effects of non-normality of the operators (Trefethen 1997), it is expected that the solution of the linear system (2.4) would tend to a multiple of the least damped eigenmode of the system as time increases. As slowly decaying solutions were found for R up to 500, the initial value calculations of Akhavan *et al.* (1991*b*) indirectly confirm the presence of weakly damped eigenmodes for this range of R. Further examination of their results indicates that the main disturbance activity in these slowly decaying perturbations was concentrated towards the centre of the channel. The eigenfunctions shown in von Kerczek & Davis (1974) and the eigenfunctions associated with the values of μ given in table 1 also have the main disturbance activity in the middle of the channel. For ease of description of the results these modes will subsequently be referred to as centre modes. A plot of $\psi_0(y)$ for a centre mode at $R=700$ is shown in figure 1; note that ψ_0 is real as μ is real. The eigenfunction for this least damped centre mode is dominated by ψ_0 with $\psi_{\pm1}$ being about one thousandth of the size of ψ_0, and monotonic decay of the size of all higher harmonics in the solution.

Despite the consistency of the three sets of results above, they give a misleading picture of the stability properties of the underlying oscillatory flow. For a channel half-width of 8, increasing the Reynolds number from 570 (see table 1) to 620 is sufficient to expose a complex μ whose real part is larger than any of the co-existing purely real eigenvalues of the system. This new mode, which is even in y, now has its main activity just outside the edge of the Stokes layer on the channel wall; the eigenfunctions found in BB also had this spatial structure. Further increases in the value of R to about 805 take this eigenvalue into the right-hand half of the complex plane, indicating linear instability of the basic flow. Similarly, when $h=16$, increasing

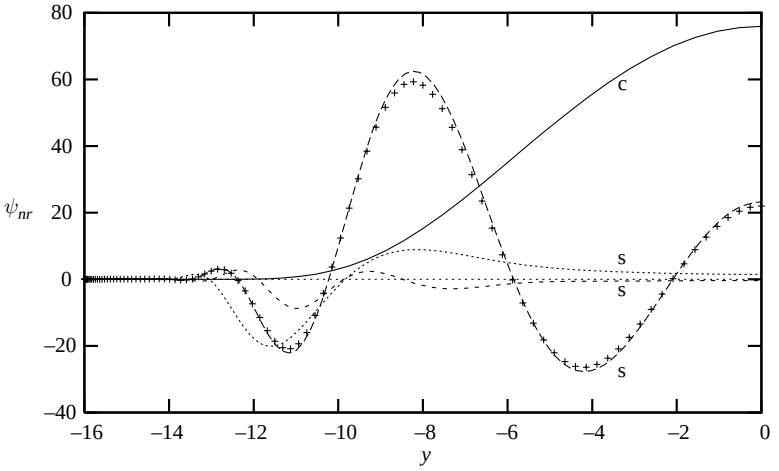

FIGURE 1. The structure of the real part of the dominant eigenfunctions, ψ_{nr}, as a function of the spatial variable y, for a centre mode and a Stokes mode at $R = 700$, $a = 0.3$ and $h = 16$. The centre mode $\psi_0(y)$ is the curve labelled c and has μ purely real with $\mu = -0.0667617$. The calculated value of μ is $\mu = -0.358467 + 0.159921\mathrm{i}$ for the Stokes mode with the real part of the eigenfunctions for $n = 0, \pm 1$ shown by the curves labelled s. The values $N = 170$ and $K = 48$ were used for the calculations shown by lines. The centre mode eigenfunction, ψ_{0r}, is shown by a solid line, with Stokes mode eigenfunctions denoted by broken lines as follows: – – – – –, ψ_{0r}; – – – – – –, ψ_{1r}; ·····, ψ_{-1r}. The + signs denote ψ_{0r} for the Stokes mode with $K = 96$.

the value of R from 750 to 760 brings out odd and even modes with complex values for μ which have real parts greater than the values given in table 1. A further increase of R to approximately 785 then makes both these even and odd travelling wave modes unstable.

The spatial structure of the larger eigenfunctions $\psi_n(y)$ making up the Stokes mode at $R = 700$ is shown in figure 1 via the curves labelled s. The difference between the spatial structure of the eigenfunctions for the least damped (even) centre mode and the even Stokes mode is quite apparent. The Stokes layer on the wall $y = -16$ of the channel extends to approximately $y = -12$ with the basic flow being almost zero in the range $-12 < y < 12$. This figure illustrates the result that for small values of n the eigenfunctions $\psi_n(y)$ are very small in the Stokes layer itself, with most of the activity occurring outside the wall layer. For higher harmonics, the maximum of the eigenfunction moves into the Stokes layer, but for these eigenfunctions the size of ψ_n is many orders of magnitude smaller than the size of ψ_0. Figure 1 also illustrates the effect of increasing the value of K on the accuracy of the eigenfunctions. The lines in this figure were produced by cubic spline interpolation of 48 data points. The points shown by a + correspond to using $K = 96$ and they agree quite well with results from the coarser mesh. Despite the fact that there is a visible difference between the values of $\psi_{0r}(y)$ for the two values of K, the computed eigenvalues μ for the two calculations agreed to six figures.

For the odd disturbance mode the dependence of the disturbance growth rate on R, for $h = 16$ and $a = 0.3$, is best seen in figure 2, which also shows the two least stable odd centre modes discussed above. Note that figure 2 pertains to odd modes; the values of μ_r for the even travelling wave (complex μ) mode would be graphically indistinguishable from the odd complex mode, despite the factor of two difference

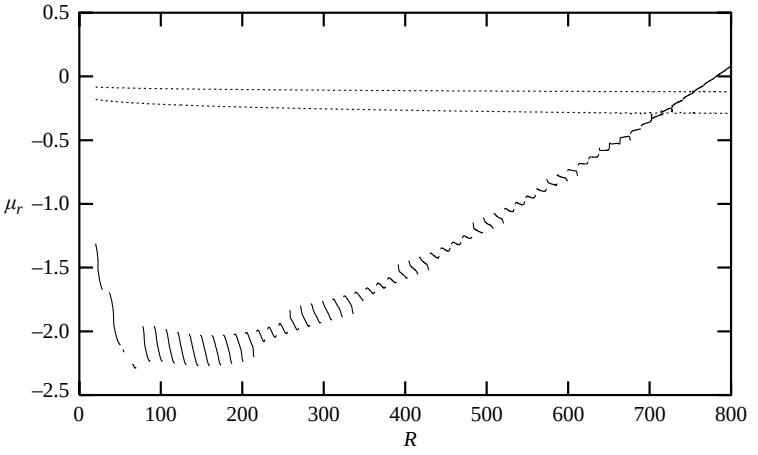

FIGURE 2. Growth rates μ_r of various odd disturbance modes, for $a = 0.3$ and $h = 16$, as a function of R. The solid lines give μ_r for the travelling wave Stokes layer disturbance mode only when μ is complex; the dashed lines give the growth rates of the first two odd centre modes.

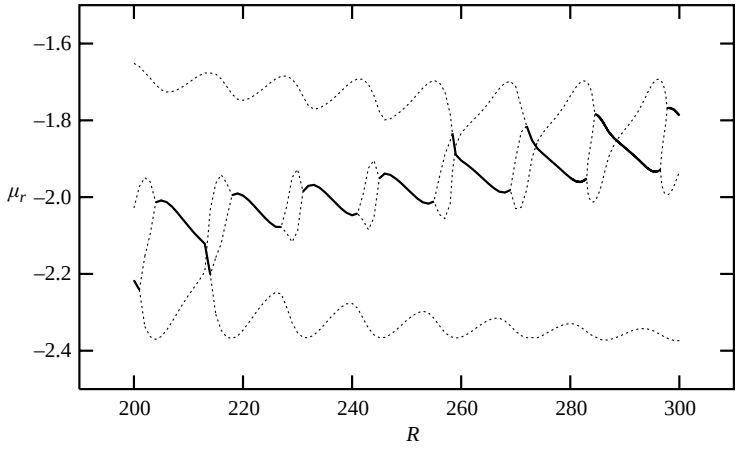

FIGURE 3. Details of the growth rate behaviour for the odd Stokes layer mode and adjacent odd centre disturbance modes as a function of R; again $h = 16$ and $a = 0.3$. The solid lines correspond to the travelling wave Stokes layer disturbance mode and indicate where μ is complex. The dashed lines correspond to purely real values of μ. Modal interaction occurs only at the end points of the solid lines.

(seen in table 1) in the growth rates for the even and odd centre modes. Further note that the growth rate behaviour of the Stokes layer mode in figure 2 has been deliberately simplified by plotting μ_r only when μ is complex; this allows a simple and direct comparison to the results shown in figure 1(b) of BB for the Stokes layer mode. For the case of the Stokes layer in a semi-infinite layer of fluid the growth rate μ took complex values on disjoint intervals of the R-axis, while between these intervals a continuous spectrum of decaying modes with $\mu_i = 0$ was allowed. In the case of Stokes layers on the walls of a wide channel, the continuous spectrum of real μ for the semi-infinite layer is replaced by a discrete spectrum of real values for the growth rate and figure 3 shows details of some of these real eigenvalues and

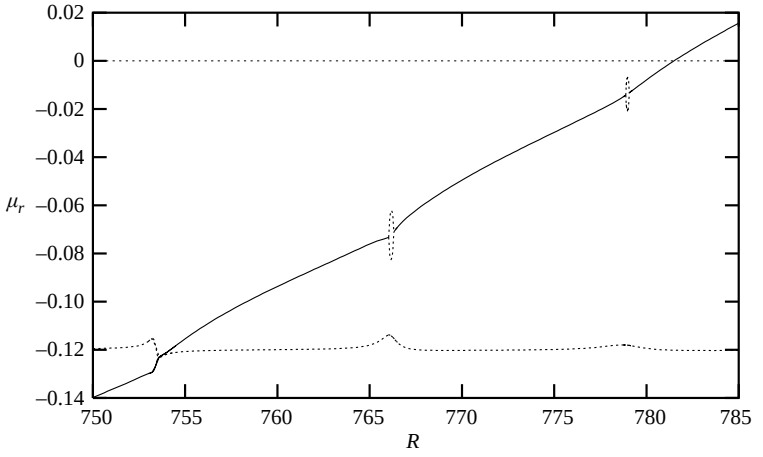

FIGURE 4. Details of growth rate variation for odd modes as a function of R near neutral conditions when $a = 0.3$ and $h = 16$. The solid lines correspond to the travelling wave Stokes layer disturbance mode and indicate where μ is complex. The dashed lines correspond to purely real values of μ.

		BB	Present results	
a	R	μ	μ^e	μ^o
0.30	800.0	(0.08174, 0.35096)	(0.08238, 0.34583)	(0.08111, 0.35610)
0.38	847.5	(0.67594, 0.14806)	(0.67616, 0.14881)	(0.67564, 0.14732)

TABLE 2. Eigenvalues μ for the semi-infinite Stokes layer, taken from BB, compared with values of μ obtained here for a wide channel ($h = 16$).

how they interact with the (eventually unstable) Stokes layer mode as the Reynolds number is increased. At the left-hand end point of each solid line in figure 3 two purely real eigenvalues combine and bifurcate to become a pair of complex-conjugate eigenvalues, corresponding to the travelling wave Stokes layer mode, as the Reynolds number is increased. The reverse process occurs at the right-hand end points of each solid line. Two complex-conjugate eigenvalues coalesce on the real axis and then separate into two purely real eigenvalues as R is increased. We remark that on the left-most and on the three solid lines towards the right of figure 3 it appears that there is mode crossing occurring at interior points away from the ends. This is purely illusory for at these points of the solid lines the imaginary part of μ is non-zero. Interactions of real and complex eigenvalues similar to those shown in figure 3 occur in all the gaps in the growth rate curve in figure 2. Further, figure 4 shows that with increasing R the complex eigenvalues continue to coalesce and split into two real eigenvalues which subsequently recombine and bifurcate to a complex-conjugate pair of eigenvalues, even when these complex eigenvalues are well away from the purely real, centre mode, part of the eigenvalue spectrum.

A more detailed check on the results for the channel was conducted by extracting some of the published values for μ from BB and comparing them with predictions from the current numerical scheme. This is presented in table 2 which shows good agreement between the values of μ from the even and odd modes for a wide channel ($h = 16$) and the growth rate for unstable modes in the semi-infinite Stokes layer. In

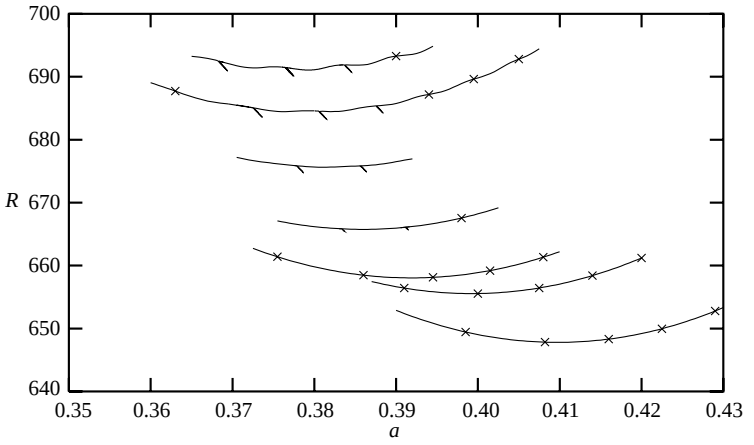

FIGURE 5. Neutral curves for even disturbance modes, around critical conditions, for h ranging from 5 to 8 in steps of one half; the lowest curve is for $h = 5$ and h increases monotonically up the figure. Some fingers are shown explicitly on the upper four curves with the crosses indicating the location of the base of the others.

particular, μ_r for the semi-infinite flow lies between the real parts of the growth rate for even and odd disturbances in the channel flow for this value of h.

The most intriguing feature of the results in BB for the semi-infinite Stokes layer was the fine structure of the neutral curve, which had thin finger-like protrusions from an essentially smooth curve (BB, figure 3). This feature was reproduced in all the neutral curves examined using the current numerical procedures. In fact the results for either the even or odd mode for a channel with $h = 16$ were essentially the same as figure 3 in BB, which concentrated on a small region, $0.368 \leqslant a \leqslant 0.386$ where $707.6 \leqslant R \leqslant 709.4$, near critical conditions on the neutral curve. The close agreement between the neutral curves for the channel flow and for the semi-infinite Stokes layer flow is not surprising as the mechanism generating the fingers is identical for both the confined and semi-infinite flow geometries under consideration. Figure 1(c) of BB shows details of two complex values of μ coalescing and then separating into two real eigenvalues as R is increased. One of these real eigenvalues moves into the right half of the complex plane for a tiny interval of R, thus forming part of a finger, before rejoining the other nearby real eigenvalue and continuing on as a complex-conjugate eigenpair with negative real part. Similar behaviour of μ for the channel flow is seen in figure 4 near $R = 778$ where the vertical, elliptical dotted parts of the growth rate curve indicate that the complex-conjugate pair of eigenvalues has been transformed into two real eigenvalues, one of which goes very close to the zero-growth-rate line. An increase of $O(10^{-3})$ in the value of a in figure 4 would cause the upper real eigenvalue to have $\mu_r > 0$ for a very narrow interval of R, and hence create a finger.

Figure 5 shows the details of the neutral curve and the associated fingers near critical conditions for even disturbance modes and channel half-widths between 5 and 8; the uppermost neutral curve is for $h = 8$. The fingers protrude from the body of the neutral curve at points where $\mu_i = 0$, as in BB, and the spacing of the fingers along the curves is fairly insensitive to the value of the channel width. However the size of each finger is very dependent on h. For $h = 8$ the fingers descend approximately 1.2 units in R from their base on the main body of the neutral curve; the base on the curve has an extent of about 4×10^{-4} units in wavenumber space. As h decreases

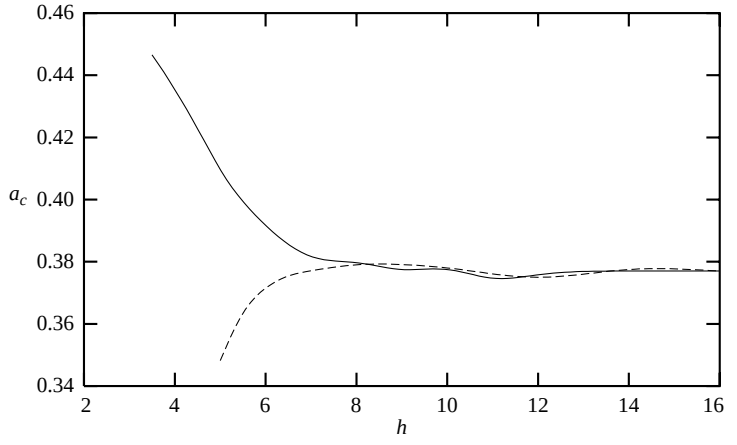

FIGURE 6. Critical wavenumber a_c as a function of channel half-width h. The solid line is for even disturbance modes while the dashed line is for odd perturbations.

both the vertical and horizontal dimensions of the fingers decrease, so that, at $h = 6.5$, the vertical drop of the fingers is barely visible on the scale of figure 5, while for $h = 5$ the base of each finger has a horizontal length of only $O(10^{-6})$ with a Reynolds number drop of approximately 0.025. The other feature evident in figure 5 is the decrease in the amplitude of the undulations of the neutral curves as h decreases. These changes in the curvature details of the neutral curve and the finger properties are due to the weakening influence of the centre modes on the Stokes layer mode as h decreases. For wide channels the centre modes are very weakly damped, as seen from table 1, and hence have significant interaction with the Stokes layer mode for Reynolds numbers close to neutral conditions. With decreasing h the centre modes become much more strongly damped and hence have much less effect on the Stokes layer mode eigenvalues near neutral conditions. Similar effects are also observed at fixed h and R well above neutral, with the value of μ_r tending to increase almost linearly with R and decreasing size of the intervals in R for which μ is purely real. Notice that the critical value of R for instability for all the values of h shown in figure 5 is associated with the tip of a finger, and hence $\mu = 0$ at critical conditions. This holds even for the tiny fingers found with $h = 5$ and is a consequence of the spacing of the fingers along the neutral curve and the small curvature of the neutral curves for flows in narrow channels. Finally, we point out that the most unstable flow configuration found for the channel occurs with h close to 5.

The variation of the linear stability critical conditions (a_c, R_c) with plate separation is shown in figures 6 and 7. (In calculating the critical conditions smoothed neutral curves were used and the effects of any protruding fingers ignored. While this is technically incorrect, this approximation causes an error of less than 0.2% in the critical Reynolds number, as the fingers extend less then 1.5 units below the bulk of the neutral curve, and will shift the critical wavenumber by less than 0.004.) Figures 6 and 7 both show that the critical conditions for oscillatory flow in a channel tend to a limiting value as the channel width increases. It is worth recalling that the critical conditions for the semi-infinite Stokes layer were given as $R_c \approx 708$ with $a_c \approx 0.375$ in BB. Thus the above figures indicate that the critical conditions for linear stability of oscillatory flow in a channel are esentially those of the semi-infinite Stokes layer for channel widths h greater than about 14. As the channel width decreases, the odd

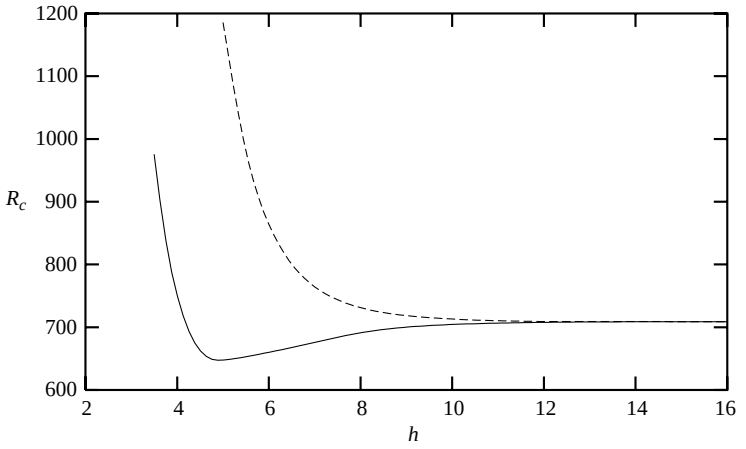

FIGURE 7. Critical Reynolds number R_c as a function of channel half-width h. The solid line is for even disturbance modes while the dashed line is for odd perturbations.

disturbance mode becomes more stable while the even mode perturbations become more unstable until $h \approx 5$, when the critical Reynolds number begins to increase. For h smaller than 5 the basic flow can no longer be described in terms of a quiescent core with Stokes layers on the walls and the basic flow velocity profile will become $U_B \sim \cos\tau + (h^2 - y^2)\sin\tau$ as $h \to 0$. Therefore at small h the basic flow is approximately quasi-steady and disturbances with properties closer to Tollmien–Schlicting waves might be expected to play a role. This will lead to an increase in the critical Reynolds number, in accordance with the results in figure 7.

Neutral curves over a wider range of wavenumber, typical of the results obtained for the stability of oscillatory channel flow, will be presented later and these will be combined with those from the analogous two-dimensional problem of axisymmetric disturbances to oscillatory flow in a circular pipe. This latter problem is considered next.

4. Axisymmetric disturbances in a pipe

Most experiments on the stability of oscillatory flow have been carried out in circular pipes, so in this section the similarity between the equations governing even disturbances in a channel and axisymmetric disturbances in a circular geometry is exploited with the aim of deriving some stability results for oscillatory flow in a pipe. The formulation of the governing equations parallels that presented for the channel stability problem given in § 2, and is only briefly outlined here. Non-dimensional coordinates (x, r, θ), with the x-axis the longitudinal axis of the pipe, are introduced, where again the lengths are scaled on a Stokes layer thickness $\sqrt{2\nu/\omega}$. The dimensionless radius of the pipe is denoted by h and with non-dimensional velocity components (u, v, w) the basic flow generated by oscillating the pipe in the direction of its longitudinal axis with velocity $U_0 \cos\omega t$ is

$$u = U_B(r, \tau) = \mathrm{Re}\left\{ \frac{J_0((1-\mathrm{i})r)}{J_0((1-\mathrm{i})h)} \mathrm{e}^{\mathrm{i}\tau} \right\} = u_1(r)\mathrm{e}^{\mathrm{i}\tau} + u_{-1}(r)\mathrm{e}^{-\mathrm{i}\tau}, \quad v = w = 0, \qquad (4.1)$$

where J_0 denotes the Bessel function of order zero. As with the channel problem, all velocity components have been scaled on U_0 and $\tau = \omega t$.

While the profile (4.1) is appropriate to the experiments of Clamen & Minton (1977), many experiments on the stability of Stokes layers are not conducted in oscillating pipes but rather in pipes held at rest while oscillatory fluid flow occurs within. If a frame of reference where the pipe walls are stationary is used then the velocity profile

$$u = U_{Bpg}(r, \tau) = \mathrm{Re}\left\{\left(\frac{J_0((1-\mathrm{i})r)}{J_0((1-\mathrm{i})h)} - 1\right)\mathrm{e}^{\mathrm{i}\tau}\right\}, \quad v = w = 0, \tag{4.2}$$

is obtained. The profile can be interpreted as being generated by a dimensional oscillatory pressure gradient $-\rho\omega U_0 \sin\omega t$, where ρ is the fluid density. It is clear that the stability properties of the basic flow profiles (4.1) and (4.2) are the same. However even the profile (4.2) is not appropriate for the piston-driven experiments of Akhavan *et al.* (1991*a*), Eckmann & Grotberg (1991) or Hino *et al.* (1976). When the basic flow is driven by a moving piston the equation of continuity requires that, for all x, the volume flux in the pipe be exactly that generated by the moving piston. This leads to the basic flow

$$u = U_{Bps}(r, \tau) = \mathrm{Re}\left\{\frac{J_0((1-\mathrm{i})h)}{J_2((1-\mathrm{i})h)}\left(1 - \frac{J_0((1-\mathrm{i})r)}{J_0((1-\mathrm{i})h)}\right)\mathrm{e}^{\mathrm{i}\tau}\right\}, \quad v = w = 0, \tag{4.3}$$

where the moving piston has (dimensional) velocity $-U_0 \cos\omega t$. It is shown in the Appendix that the stability properties of the piston-driven basic flow (4.3) are simply related to those of the wall-driven flow (4.1). In particular, if the flow (4.1) is neutrally stable at the wave number $a^\dagger$ and Reynolds number $R^\dagger$ then the flow (4.3) is also neutrally stable at the same wavenumber but at the lower Reynolds number $|J_2((1-\mathrm{i})h)/J_0((1-\mathrm{i})h)|R^\dagger$. Thus it is only necessary to examine the stability of the basic state given by (4.1) in order to cover most of the conditions that have been used in experiments. Note that the factor $|J_2((1-\mathrm{i})h)/J_0((1-\mathrm{i})h)|$ is about 0.9 at $h = 10$ and tends to 1 as $h \to \infty$; its value has been ignored, and will continue to be ignored, in our discussions of experimental results.

For axisymmetric disturbances the perturbed velocity is given by

$$(u, v, w) = (U_B, 0, 0) + \varepsilon\left(\frac{1}{r}\frac{\partial\Psi}{\partial r}, -\frac{1}{r}\frac{\partial\Psi}{\partial x}, 0\right), \tag{4.4}$$

where $\varepsilon \ll 1$ and $\Psi(x, r, \tau)$ denotes the stream function, which is further decomposed as

$$\Psi = \mathrm{e}^{\mu\tau}\mathrm{e}^{\mathrm{i}ax}\psi(r, \tau) + \text{complex conjugate}; \tag{4.5}$$

$\psi(r, \tau)$ is taken to be 2π-periodic in τ. With this form for the velocity field the linearized equation for ψ is then

$$\frac{\partial}{\partial\tau}(\mathscr{D}^2 - a^2)\psi = \left\{\tfrac{1}{2}(\mathscr{D}^2 - a^2) - \mu - \mathrm{i}aRU_B\right\}(\mathscr{D}^2 - a^2)\psi + \mathrm{i}aR(\mathscr{D}^2 U_B)\psi, \tag{4.6}$$

subject to

$$\psi = \psi_r = 0 \quad \text{on} \quad r = h. \tag{4.7}$$

Here the operator $\mathscr{D}^2$ is given by $\mathscr{D}^2 = r\partial_r(r^{-1}\partial_r)$ as usual. From this point the derivation of the discrete equations analogous to (2.7) follows that for the channel so closely that the analysis is not replicated here. The only changes of substance are the new definitions of the differentiation matrices $\boldsymbol{L}$ and $\boldsymbol{V}$ associated with the use of polar coordinates and the replacement of the U_{Byy} coefficient by the quantity $\mathscr{D}^2 U_B$. Thus (2.7) is also the discrete equation governing the stability of the pipe flow

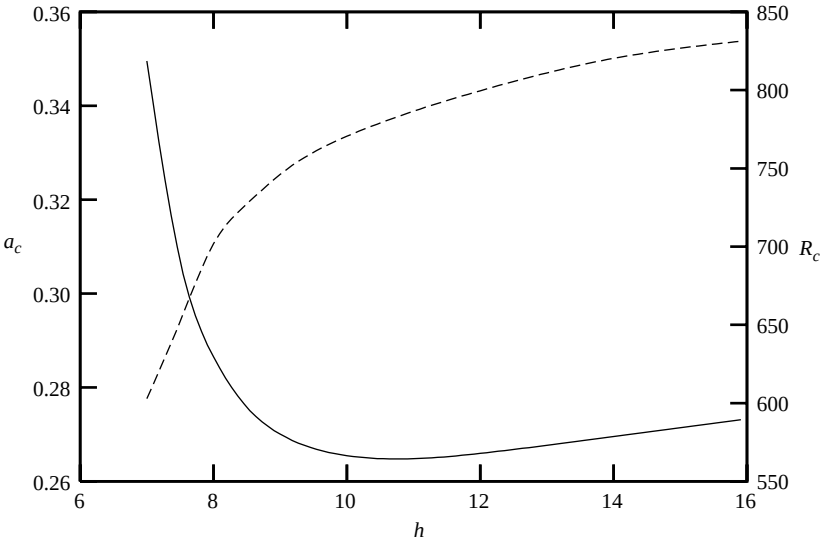

FIGURE 8. Critical conditions for instability in a pipe as a function of pipe radius h. The solid line gives R_c and the dashed line gives a_c.

provided that $\boldsymbol{L}$, $\boldsymbol{V}$ and $\boldsymbol{M}$ are now given by

$$\left(\partial_r^4 - 2r^{-1}\partial_r^3 + (3r^{-1} - 2a^2)\partial_r^2 - (3r^{-3} - 2r^{-1}a^2)\partial_r + a^4\right)/2 \to \boldsymbol{V}, \tag{4.8a}$$

$$\partial_r^2 - r^{-1}\partial_r - a^2 \to \boldsymbol{L} \quad \text{and} \quad \boldsymbol{M} = \boldsymbol{L}^{-1}(u_1\boldsymbol{L} - u_{1L}\boldsymbol{I}), \tag{4.8b}$$

where u_{1L} denotes the diagonal matrix with values at the mesh points given by

$$u_{1L} = -\mathrm{i}\frac{J_2((1-\mathrm{i})r)}{J_0((1-\mathrm{i})h)}. \tag{4.8c}$$

Last, allowing some abuse of notation again, within the definition of $\boldsymbol{M}$, u_1 denotes the square matrix with the mesh values of $u_1(r)$ down the diagonal. Following Fornberg (1996) a Chebyshev mesh was applied to the diameter of the pipe and the even symmetry appropriate to axisymmetric solutions used to reduce the computational domain to $0 \leqslant r \leqslant h$. The kinematic conditions at the origin (Batchelor & Gill 1962) required $\psi_n(0) = 0$ for axisymmetric solutions and the usual no-slip conditions were imposed at the pipe wall using the same techniques as for the channel. The eigenvalue problem (2.10) was again obtained following the assembly of the $\boldsymbol{\psi}_n$ into the vector $\boldsymbol{\Phi}$ in the manner of (2.11).

The eigenvalues of (2.10) now determine the properties of axisymmetric disturbances in purely oscillatory pipe flow. Matlab was again used to find the eigenvalues and eigenvectors of (2.10) and checks similar to those described for the channel calculations were applied to the results of these pipe flow calculations. In particular, at low R the results obtained for μ agreed with the circular-pipe analogue of the Dolph–Lewis eigenvalues, indicating that the differentiation matrices for the Laplacian and viscous operators in (4.8) had been correctly implemented. The variation of μ with R and a for the pipe flow exactly parallels that obtained for the even modes in the channel, so little discussion of the qualitative features of the behaviour is needed. Instead the main results are given immediately.

The variation with h of the critical conditions (a_c, R_c) for instability in a pipe is shown in figure 8. This figure shows that for oscillatory flow in a pipe there is an

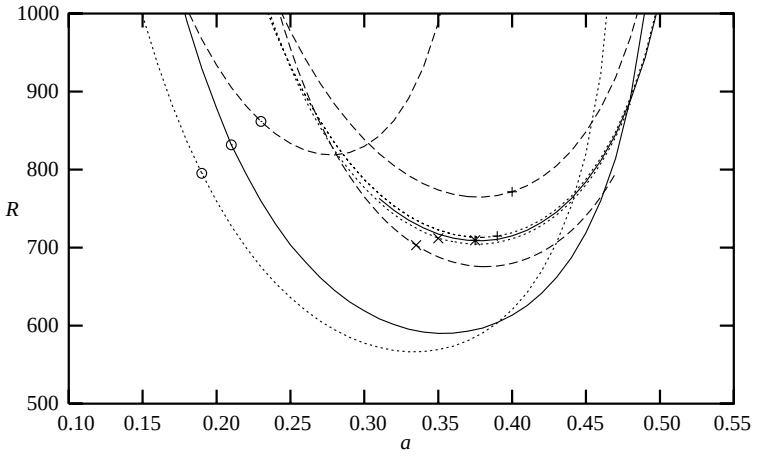

FIGURE 9. Neutral curves for even and odd disturbance modes in a channel and for axisymmetric perturbations in a pipe. The circle symbol labels the pipe neutral curves, the $\times$ symbol the even channel modes with $+$ attached to the odd channel mode neutral curves. The solid lines are for $h = 16$, the dotted lines for $h = 10$ and the dashed lines for $h = 7$.

overall minimum in R_c at a pipe radius of about 11. This pipe radius is very close to that used by Akhavan *et al.* (1991*a*) in their experiments and further comparison with their results will be given in the conclusions. Although not shown in this figure, for values of pipe radius greater than about 25 the critical conditions for axisymmetric disturbances in the pipe tend to the critical conditions for even (or odd) disturbances in a channel, and hence to the critical conditions for the Stokes layer in a semi-infinite flow. Recall that in the channel the minimum R_c occurred at $h \approx 5$ with agreement between R_c for the channel and the semi-infinite flow appearing for h greater than about 14. This factor of approximately two difference in the values of h for the salient features of R_c in a pipe and in a channel is removed if the geometry of the flow domain is characterized by an area measure rather than a linear measure. The ratio of the area of the flow domain to the area occupied by the Stokes layer in the channel is just $2h/2 = h$, while in the pipe this same area ratio is now $(\pi h^2/2\pi h) = h/2$, to leading order. Thus to achieve the same area ratio in a pipe as in a channel, the radius of the pipe needs to be approximately double the half-width of the channel.

Finally a collection of smoothed neutral curves, for various values of h, for both the channel and the pipe is shown in figure 9. For the channel, the even and odd mode neutral curves are indistinguishable at $h = 16$ so there appears to be only one full line for the channel in figure 9. This neutral curve is bracketed by the dotted lines corresponding to the neutral curves at $h = 10$, with the lower curve associated with the even mode disturbance. When $h = 7$ the stability properties of the even and odd modes are now quite different and their neutral curves are well separated, again with the even mode curve being the lower dashed line. The neutral curves for the circular pipe, at the same values of h as for the channel, are labelled with a circle. The dotted curve at $h = 10$ has a critical R of about 566, which is close to the minimum $R_c(h)$ given in figure 8.

The results in figure 9 are for the wall-driven flow (4.1) or the pressure-gradient-driven flow (4.2). If we were to consider the piston-driven oscillatory flow (4.3) then only the labelling on the Reynolds number axis of figure 9 would need to be changed.

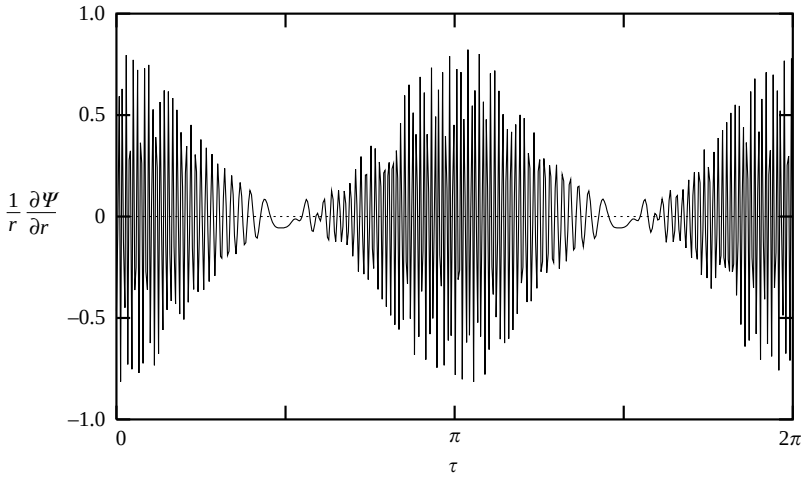

FIGURE 10. Arbitrarily scaled axial velocity perturbation in a pressure-gradient-driven flow at $r = 8.4095$, with $R = 540$, $a = 0.33347$ and $h = 10.6$.

In particular, for a piston-driven oscillatory flow in a pipe with $h = 10$ the critical value of R would be reduced to approximately $0.9 \times 566 \approx 510$.

5. Discussion and conclusions

The most encouraging aspect of the neutral curves presented in figure 9 is that, over a range of pipe radii, the theoretically predicted critical Reynolds number for linear instability is closer to the experimentally observed transition to turbulence occurring at Reynolds numbers of about 250 to 275 than the corresponding results for a channel flow. Nevertheless, there is of course still a large discrepancy between the experimental observations and the calculations presented here. As just one example, Akhavan *et al.* (1991*a*) examine the structure of the turbulent, purely oscillatory, piston-driven flow in a pipe with $h = 10.6$ and $R = 540$, while according to our calculations, the flow would only be just linearly unstable. Similarly, figure 6 in Eckmann & Grotberg (1991) displays turbulent velocity measurements at $R = 427$ with $h \approx 20$ while our results indicate that the flow is linearly stable.

Most reports of experiments on the stability of purely oscillatory flow present velocity traces, either from laser-Doppler devices (Akhavan *et al.* 1991*a*; Eckmann & Grotberg 1991) or from hot-wire anemometers (Eckmann & Grotberg 1991; Hino *et al.* 1976), at a selection of fixed positions inside the pipe. Equations (4.4) and (4.5) define the axial velocity component, and in figure 10 the arbitrarily scaled predicted axial velocity perturbation at $r = 8.4095$ for the least damped mode with $R = 540$ and $h = 10.6$ is shown for one cycle of the basic flow. The apparent resemblance of this velocity-versus-time trace to turbulent bursts in the flow is noted. The displayed velocity trace comes from the eigenfunction corresponding to the eigenvalue $\mu = -0.105574$ where $a = 0.33347$ and the pressure-gradient-driven basic flow given by (4.2). The parameter h was chosen to be close to one set of the experimental conditions examined by Akhavan *et al.* (1991*a*), R was chosen to be slightly below critical for a wall-driven or pressure-gradient-driven flow. Further, a was selected to be close to the appropriate critical wavenumber and, for convenience, so that μ was purely real. The velocity trace displayed in figure 10 indicates the axial velocity

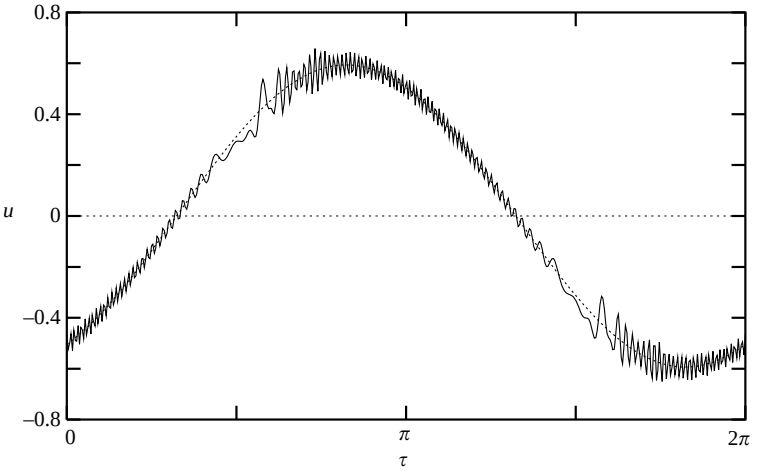

FIGURE 11. Axial velocity variation with time in a pressure-gradient-driven flow at $r = 10.0375$, with $R = 540$, $a = 0.33347$ and $h = 10.6$. The size of the perturbation velocity has been chosen arbitrarily to make the fluctuations visible. The dashed curve is the undisturbed axial velocity.

perturbation occurring just outside the edge of the Stokes layer on the pipe wall. Note that the exponential decay of the velocity perturbation in time has been suppressed in plotting this figure; in other words the $e^{\mu\tau}$ part in the stream function decomposition (4.5), with μ real-valued, has not been shown.

The variation with time of the axial velocity inside the Stokes layer plotted in figure 11 shows the combined effect of superimposing the disturbance onto the underlying basic profile. The size of the velocity perturbation has been arbitrarily set to make the perturbations visible and again the decay in time of the perturbation has been ignored. Here $r = 10.0375$, but all other parameters are as in figure 10. Allowing for the rectification of the velocity inherent in hot-wire anemometry this velocity trace looks similar to those reported by Hino *et al.* (1976) and Eckmann & Grotberg (1991).

The extremely high-frequency components in this laminar velocity distribution are actually nothing more than artifacts of the choice of reference frame for the basic flow. With the basic flow (4.1) and identical values for the parameters a, R and h the numerical solution of the governing equation (4.6) again gives the eigenvalue $\mu = -0.105774$, but this time a much simpler eigenfunction results and the velocity trace corresponding to figure 10 is now as shown in figure 12. The effect of a change in frame of reference for the basic flow was noted in BB, and here it is easy to show that if equation (4.5) gives the form of the stream function for a wall-driven basic flow, with $\psi(r, \tau)$ the solution of equation (4.6), then the stream function for the pressure-gradient-driven basic flow becomes

$$e^{\mu\tau} e^{iax} e^{iaR\sin\tau} \psi(r, \tau) + \text{complex conjugate}, \tag{5.1}$$

with the same μ and ψ as in equation (4.5). Thus the high-frequency oscillations in the velocity signal are due to the presence of the $e^{iaR\sin\tau}$ term in (5.1), while the apparent bursts of activity in figure 10 are just the result of the points of stationary phase in the $e^{iaR\sin\tau}$ factor. We reiterate that the slow exponential decay in time, the $e^{\mu\tau}$ term, has been omitted from the velocity traces in both figures 10 and 12.

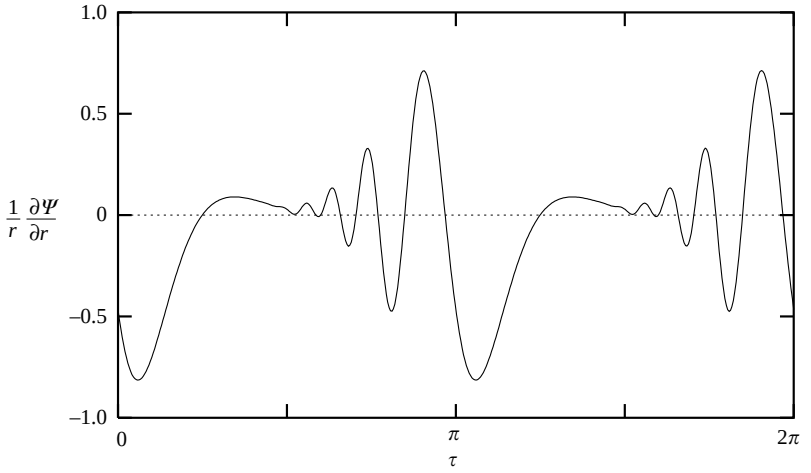

FIGURE 12. Arbitrarily scaled axial velocity perturbation in a wall-driven flow at $r = 8.4095$, with $R = 540$, $a = 0.33347$ and $h = 10.6$.

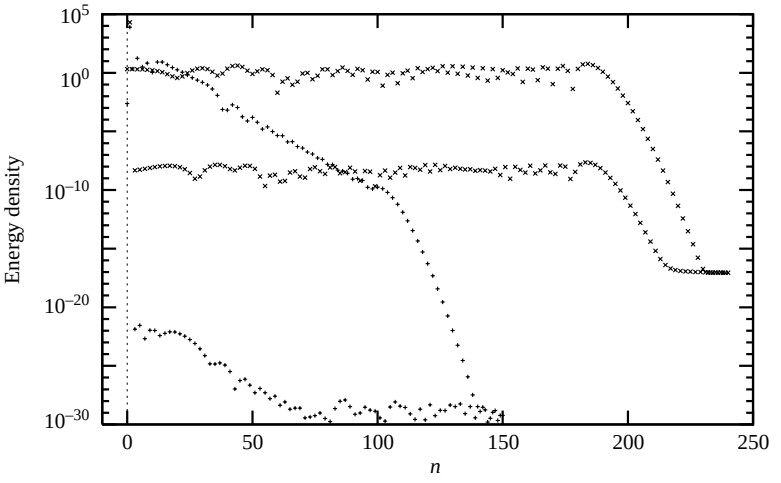

FIGURE 13. Energy density spectrum for the axial velocity variation with time in a pressure-gradient-driven flow ($\times$) and a wall-driven flow ($+$) at $r = 10.0375$, with $R = 540$, $a = 0.33347$ and $h = 10.6$.

The velocity trace shown in figure 11 can be decomposed into its harmonic components, resulting in the energy density spectrum shown by the $\times$ symbols in figure 13. The $n = 1$ component, the basic flow, contains the most energy and, apart from this odd harmonic, the even harmonics denoted by the upper set of $\times$ symbols contain nearly 8 orders of magnitude more energy than the odd harmonics. The energy is spread evenly over the even harmonics for n up to about 200 and then there is a rapid decrease in energy density with increasing n. The flat section of the spectrum around the energy density of 10^{-15} is associated with the previously mentioned numerical difficulties in determining the eigenfunction. The $+$ symbols denote the energy density spectrum of a velocity trace when the basic flow is generated by oscillating the pipe itself. The value of $r = 10.0375$, when $h = 10.6$, has ensured that the amplitude of the basic flow is approximately the same for the two flow configurations, and this is

reflected in the energy density levels agreeing approximately for the $n = 1$ frequency. Again, the even harmonics contain the majority of the energy of the perturbation, but the bandwidth of frequencies in the disturbance is much smaller when the pipe oscillates. This is primarily due to not having to represent the function $e^{iaR\sin\tau}$ as a Fourier series.

Apart from Clamen & Minton (1977), all the experimental work discussed here has effectively used a pressure-gradient-driven basic flow and all report high-frequency oscillations in the velocity traces for a range of quite small Reynolds numbers. However, these perturbed velocity traces are uniformly described in terms of some type of turbulence. For instance, Hino *et al.* (1976) use the term "weakly turbulent" to describe a flow where the velocity traces contain high-frequency components, but otherwise have good agreement with the theoretical basic flow. A flow with R as small as 35, for $h = 6.19$, is then classified as weakly turbulent by those authors. However, an alternative explanation is that the mechanical vibrations associated with the production of linear oscillatory motion from rotational motion, via some form of scotch yoke, periodically forces the damped modes of the system. Eckmann & Grotberg (1991) acknowledge the presence of periodic, mechanical vibrations in the drive mechanism used in their experiments and it is likely that all the experiments discussed here suffer from some level of external vibration. The structure (5.1) of small disturbances in pressure-gradient-driven flows applies to the weakly damped centre modes as well as the Stokes mode and hence it could be possible to observe decaying, highly oscillatory perturbations in each cycle at low Reynolds numbers. Thus, at $h = 2.76$ and $R = 193$ the velocity trace in figure 4(a) of Hino *et al.* (1976) is entirely consistent with an interpretation as a laminar, high-frequency perturbation, rather than their identification of the flow as weakly turbulent. Similarly, Eckmann & Grotberg (1991) explain the large scatter in their laser-Doppler velocity measurements at $R = 427$ in terms of turbulence in the Stokes layer on the wall. Given the structure (5.1) of the disturbances, this conclusion can now be questioned as the sampling rate of the velocity was only 100 measurements per cycle while approximately $2aR$ samples per cycle would be needed to resolve the highest frequency components in the velocity. Further, with wavenumbers around 0.3, a sampling rate of about 250 measurements per cycle is needed when $R = 427$. A similar observation can be made on the experiments reported by Akhavan *et al.* (1991a) who conducted a large number of experiments with $R = 540$ and a sampling rate of 240 measurements per cycle which is again below the Nyquist frequency.

The presence of these high-frequency oscillations in the disturbance structure associated with pressure-gradient-driven flow will certainly make experimental determination of critical conditions difficult, but our results reveal a further, unexpected complication for experimental work. For the experiments discussed here critical conditions were determined by comparing measured velocity profiles with the velocity profile appropriate to oscillatory flow in an infinitely long pipe. If there were significant differences between the theoretical predictions and the observed axial velocity then the basic flow was considered to be in the unstable flow regime. Underlying this approach is the assumption that any flow disturbances caused by the driving piston, or a contraction in the pipe, will decay with distance away from the piston, or the contraction, leaving a velocity profile close to that in an infinitely long pipe. Eckmann & Grotberg (1991) quote Gerrard & Hughes (1971) as the source for the entrance length formula $L = 0.06DR$ (in our scaling) to justify their claims that their test section is free of any inlet effects. Here D is the (dimensional) pipe diameter and Eckmann & Grotberg (1991) had a worst case L/D of approximately 29; the

apparatus of Akhavan *et al.* (1991*a*) had $L/D = 400$ while that of Hino *et al.* (1976) had L/D values as low as 70.

In principle, the nonlinear equations and boundary conditions governing the laminar, axisymmetric flow generated by a piston performing axial oscillations in a long pipe of constant cross-section are straightforward to write down. The exact solution of these equations is of course extremely difficult to obtain, but the main features of the flow are easily inferred. Close to the piston we expect the axial velocity to be purely oscillatory and almost uniform over the cross-section, apart from a thin boundary layer on the walls of the pipe, with significant oscillatory radial velocity components. Further from the driving piston we would expect reduced radial velocity components as the velocity field approached the purely axial form (4.2). Sufficiently far from the piston, the nonlinear equations governing the basic flow can be approximated by linear equations which describe the ultimate approach to this purely axial velocity field. If the spatial decay of the remnant effects of the driving piston is sought via a stream function of the form

$$\int_0^r sU_{Bps}(s, \tau)\,\mathrm{d}s + \mathrm{e}^{\mathrm{i}ax}\mathrm{e}^{\mu\tau}\Psi(r, \tau)$$

then equation (4.6) is obtained provided provided $\|\Psi\| \ll 1$. As we are describing the basic flow we must have $\mu_r = 0$ and for the spatial decay of the synchronous components of the effects of the piston we require $\mu_i = 0$, making $\mu = 0$ in (4.6). Thus the ultimate spatial decay of disturbances due to an oscillating piston hinges on the existence of eigenvalues a with $a_i > 0$. Unfortunately, our result that $\mu = 0$ at the critical conditions for instability now has the additional implication that perturbations in the basic flow, caused by imperfections in the experimental apparatus, do not decay spatially at critical conditions. As a is real at critical conditions, the $\mathrm{e}^{\mathrm{i}ax}$ term in the disturbance structure (4.5) does not produce any spatial decay with changes in x. Thus our linear stability predictions also mean that the method of experimentally determining critical conditions described above is not valid as the effects of the oscillating piston (or pipe contraction) extend further and further from the piston as the critical Reynolds number is approached. This conclusion merits some qualification however, for although $\mu = 0$ at critical conditions, this only occurs on the protruding fingers of the neutral curve. It could be argued that the fingers are so tiny that other nearby parts of the neutral curve, on which $\mu_i \neq 0$, could be determined experimentally provided that one can suppress the initial disturbance to a sufficiently low level.

At low Reynolds numbers it is possible to calculate the complex eigenvalues a for any of the basic flows (4.1)–(4.3) when μ is purely imaginary. There are several families of eigenmodes present for small R, but it can be shown that the least spatially damped disturbances have a wavenumber expansion in the form

$$\mathrm{i}ah \sim -j_{1,1} + O\left(n^{-1/2}, R\right) \quad \text{where } n \to \infty \text{ and } R \to 0. \tag{5.2}$$

Here $j_{1,1}$ is the first positive zero of the Bessel function $J_1(z)$ and n denotes the harmonic in the expansion $\psi(r, \tau) = \sum_{n=-\infty}^{\infty} \psi_n(r)\mathrm{e}^{\mathrm{i}n\tau}$. Thus, at low Reynolds numbers, all synchronous disturbances will have decayed spatially by at least a factor of e when x/h increases by approximately 0.26.

Some preliminary calculations using the Matlab routine `polyeig`, for values of R up to 5 and with $\mu = 0$, showed a complicated evolution of the eigenvalues for a. The behaviour of the values for a was somewhat similar to that observed for the evolution of μ as R was increased, allowing for the fact that the values for a are close to the imaginary axis while those for μ were near the real line. Extending the calculation

of the eigenvalues for a to larger values of R was not feasible, and in any event the answers are already known. For example with the basic flow (4.1) then at $R \approx 566.4$ and $h = 10$ the eigenvalue for a will be purely real with $a \approx 0.3335$.

While our results for the stability of oscillatory flow in a channel or pipe do not agree with the current experimentally accepted Reynolds number for the transition from laminar flow to turbulent flow, we have provided independent confirmation of the original predictions made in BB for the stability of a Stokes layer on a flat plate.† The present results also suggest that the many experimental measurements of high-frequency disturbances in oscillatory pipe flow may have been misinterpreted as evidence of turbulent bursts in the flow, when in fact the flow is still completely laminar. Further, our results show that the usual assumption regarding the spatial decay of entry length effects does not necessarily hold in oscillatory flows, providing yet more difficulties in the experimental determination of the transition to turbulence.

The above comparison of experimental observations with our results, based on two-dimensional, linear, Floquet theory is only one of several possible interpretations of the existing experimental results. Other scenarios describing the stability properties of oscillatory flow bring in three-dimensional effects or nonlinear effects. Within the context of linear theory, Squire's theorem allows us to consider only two-dimensional eigenmodes, as we have done in this paper, but there is no guarantee that two-dimensional initial value formulations of the stability problem will capture the often stated explosive growth of small disturbances during the deceleration phase of the velocity cycle. Indeed, the two-dimensional numerical results of Akhavan *et al.* (1991*b*) found no such rapid growth of disturbances in their initial value calculations. Thus, for two-dimensional disturbances it appears that nonlinear effects would need to be invoked to explain the cyclic rapid growth of small perturbations. Under the assumption that nonlinear effects produce finite growth rates, our linear theory results should be recoverable experimentally provided that background disturbances are kept so small that, even with the nonlinear growth effects in play, the disturbance size remained sufficiently small for linear theory to hold throughout the entire cycle. Whether this can be achieved in real experiments is of course open to question and obviously limits the practical application of our theory.

Quasi-steady theory suggests that when $R \gg 1$ the instantaneous growth rate of disturbances is $O(R)$ so that over an $O(1)$ time an initial perturbation might amplify by a factor of $O(\exp(\gamma R))$ for some $O(1)$ constant γ. Continuing this argument it might appear that linearization is therefore only justifiable if the disturbance amplitude is exponentially small. While this result is only formally valid for $R \to \infty$, if it continues to hold for finite R then it could impose a severe restriction on experiments. However calculations described in Akhavan *et al.* (1991*b*) imply that at $R = 500$ the largest instantaneous growth rate is only $O(10^{-2})$ and certainly nowhere near the $O(R)$ size suggested by quasi-steady theory. Thus the conclusion that linearization might only be valid for exponentially small perturbations appears to be unduly pessimistic.

The available direct numerical solutions of the governing Navier–Stokes equations for oscillatory flow consider two-dimensional flows (Juárez & Ramos 2003) and

† Since completing this work we have learnt of calculations by Gao & Lu (2006) which provide further independent confirmation of some of the predictions in BB. They were concerned with the effects of wall suction and blowing on the stability of the flat Stokes layer and although their numerical scheme was similar in spirit to that used in BB, it was independently developed. In all cases where direct comparison could be made their results show excellent agreement with those in BB.

two- and three-dimensional flows in channels (Cosgrove, Buick & Tonge 2003). Neither are easily related to our calculations, but they both report turbulence at values of Reynolds number where our results indicate the basic flow to be stable. However, the results of Juárez & Ramos (2003) at $R = 268.5$ do show an almost uni-directional, laminar flow field at one time instant with a distorted, vortical field at some later time in the cycle. This is consistent with a scenario of laminar, high-frequency oscillations occuring periodically while the underlying flow is still stable, as discussed above. Clearly there is still scope for much further work on the stability properties of purely oscillatory flows.

We thank the referees for their comments and suggestions for improvement of this paper.

Appendix. Stability of a generic oscillatory flow in a pipe

Here we provide some further evidence on the relationships between the stability properties of the basic flows (4.1)–(4.3). Both velocity profiles (4.2) and (4.3) have the general form

$$U(r,\tau) = \mathrm{Re}\left\{ A\left(\frac{J_0((1-\mathrm{i})r)}{J_0((1-\mathrm{i})h)} - 1 \right) \mathrm{e}^{\mathrm{i}\tau} \right\}, \quad v = w = 0, \tag{A 1}$$

where the constant $A = 1$ for the pressure-gradient-driven flow given by (4.2) and $A = -J_0((1-\mathrm{i})h)/J_2((1-\mathrm{i})h)$ for the oscillating piston case (4.3). The generic form $U(r,\tau)$ in (A 1) can be written in terms of $U_B(r,\tau)$ (as defined by (4.1)) according to

$$U(r,\tau) = |A| U_B(r, \tau+\alpha) - |A| \cos(\tau+\alpha) \tag{A 2}$$

where $\alpha = \arg\{A\}$. The equation governing the stability of the profile $U(r,\tau)$ is (4.6) with U_B, $\psi(r,\tau)$, μ and R replaced by U, $\phi(r,\tau)$, μ_g and R_g respectively. Explicitly, the equation becomes

$$\frac{\partial}{\partial\tau}(\mathscr{D}^2 - a^2)\phi = \left\{ \tfrac{1}{2}(\mathscr{D}^2 - a^2) - \mu_g - \mathrm{i}aR_g U \right\}(\mathscr{D}^2 - a^2)\phi + \mathrm{i}aR_g(\mathscr{D}^2 U)\phi, \tag{A 3}$$

subject to

$$\phi = \phi_r = 0 \quad \text{on} \quad r = h. \tag{A 4}$$

By replacing the generic profile U with its representation in terms of U_B, equation (A 3) can be recast as

$$\begin{aligned} \frac{\partial}{\partial\tau}(\mathscr{D}^2 - a^2)\phi = {} & \tfrac{1}{2}(\mathscr{D}^2 - a^2)^2\phi - \mu_g(\mathscr{D}^2 - a^2)\phi - \mathrm{i}aR_g|A|U_B(r,\tau+\alpha)(\mathscr{D}^2 - a^2)\phi \\ & + \mathrm{i}aR_g|A|\cos(r,\tau+\alpha)(\mathscr{D}^2 - a^2)\phi + \mathrm{i}aR_g|A|(\mathscr{D}^2 U_B(r,\tau+\alpha))\phi. \end{aligned} \tag{A 5}$$

Suppose that $\psi(r,\tau)$ denotes the eigensolution of (4.6) corresponding to the eigenvalue μ at parameter values R and a. If we now set

$$\phi(r,\tau) = \mathrm{e}^{\mathrm{i}aR_g|A|\sin(\tau+\alpha)}\psi(r,\tau+\alpha) \tag{A 6}$$

in (A 5) the stability of the generic profile (A 1) is now governed by the problem

$$\frac{\partial}{\partial\tau}(\mathscr{D}^2 - a^2)\psi = \left\{ \tfrac{1}{2}(\mathscr{D}^2 - a^2) - \mu_g - \mathrm{i}aR_g|A|U_B \right\}(\mathscr{D}^2 - a^2)\psi + \mathrm{i}aR_g|A|(\mathscr{D}^2 U_B)\psi, \tag{A 7}$$

with boundary conditions

$$\psi = \psi_r = 0 \quad \text{on} \quad r = h, \tag{A 8}$$

where all terms are evaluated at $\tau + \alpha$. As the origin of time is immaterial here, the above problem is identical to (4.6) provided we take $R = |A|R_g$ and $\mu = \mu_g$. Thus the stability properties of the basic flows (4.2) and (4.3) can be deduced from knowledge of the stability properties of the wall-driven flow (4.1).

REFERENCES

Akhavan, R., Kamm, R. D. & Shapiro, A. H. 1991*a* An investigation of transition to turbulence in bounded oscillatory Stokes flows. Part 1. Experiments. *J. Fluid Mech.* **225**, 395–422.

Akhavan, R., Kamm, R. D. & Shapiro, A. H. 1991*b* An investigation of transition to turbulence in bounded oscillatory Stokes flows. Part 2. Numerical simulations. *J. Fluid Mech.* **225**, 423–444.

Batchelor, G. K. & Gill, A. E. 1962 Analysis of the stability of axisymmetric jets. *J. Fluid Mech.* **14**, 529–551.

Blennerhassett, P. J. & Bassom, A. P. 2002 The linear stability of flat Stokes layers. *J. Fluid Mech.* **464**, 393–410 (referred to herein as BB).

Clamen, M. & Minton, P. 1977 An experimental investigation of flow in an oscillating pipe. *J. Fluid Mech.* **77**, 421–431.

Conrad, P. W. & Criminale, W. O. 1965 The stability of time-dependent laminar flow: parallel flows. *Z. Agnew. Math. Phys.* **16**, 233–254.

Cosgrove, J. A., Buick, J. M. & Tonge, S. J. 2003 Evolution of turbulence in an oscillatory flow in a smooth-walled channel: A viscous secondary instability mechanism. *Phys. Rev.* E **68**, 026302.

Cowley, S. J. 1987 High frequency Rayleigh instability analysis of Stokes layers. In *Stability of Time-dependent and Spatially Varying Flows* (ed. D. L. Dwoyer & M. Y. Hussaini), pp. 261–275. Springer.

Dolph, C. L. & Lewis, D. C. 1958 On the application of infinite systems of ordinary differential equations to perturbations of plane Poiseuille flow. *Q. Appl. Maths* **16**, 97–110.

Eckmann, D. M. & Grotberg, J. B. 1991 Experiments on transition to turbulence in oscillatory pipe flow. *J. Fluid Mech.* **222**, 329–350.

Fornberg, B. 1996 *A Practical Guide to Pseudospectral Methods*. Cambridge University Press.

Gao, P. & Lu, X.-Y. 2006 Effects of wall suction/blowing on the linear stability of flat Stokes layers. *J. Fluid Mech.* **551**, 303–308.

Gerrard, J. H. & Hughes, M. D. 1971 The flow due to an oscillating piston in a cylindrical tube: a comparison between experiment and a simple entrance flow theory. *J. Fluid Mech.* **50**, 97–106.

Hale, J. F., McDonald, D. A. & Womersley, J. R. 1955 Velocity profiles of oscillating arterial flow with some calculations of viscous drag and the Reynolds number. *J. Physiol.* **128**, 629–640.

Hall, P. 1978 The linear stability of flat Stokes layers. *Proc. R. Soc. Lond.* A **359**, 151–166.

Hall, P. 2003 On the stability of Stokes layers at high Reynolds numbers. *J. Fluid Mech.* **482**, 1–15.

Hino, M., Sawamoto, M. & Takasu, S. 1976 Experiments on transistion to turbulence in oscillatory pipe flow. *J. Fluid Mech.* **75**, 193–207.

Juárez, L. H. & Ramos, E. 2003 Direct numerical simulation of transition to turbulence in an oscillatory channel flow. *C. R. Méca.* **331**, 55–60.

von Kerczek, C. & Davis, S. H. 1974 Linear stability theory of oscillatory Stokes layers. *J. Fluid Mech.* **62**, 753–773.

Ku, D. N. 1997 Blood flow in arteries. *Annu. Rev. Fluid Mech.* **29**, 399–434.

Selverov, K. P. & Stone, H. A. 2001 Peristaltically driven channel flows with applications towards micro-mixing. *Phys. Fluids* **13**, 1837–1859.

de Souza, M. O. 1998 Instabilities of rotating and unsteady flows. PhD thesis, University of Cambridge.

Suresh, V. & Homsy, G. M. 2004 Stability of time-modulated electro-osmotic flow. *Phys. Fluids* **16**, 2349–2356.

Trefethen, L. N. 1997 Pseudospectra of linear operators. *SIAM Rev.* **39**, 383–406.

Trefethen, L. N. 2000 *Spectral methods in MATLAB*. Philadelphia, PA: SIAM.